ChemPhysChem

Research Article
doi.org/10.1002/cphc.202300409

Chemistry Europe
European Chemical
Societies Publishing

www.chemphyschem.org

CO$_2$ and H$_2$ Activation on Zinc-Doped Copper Clusters

Bárbara Zamora,[a] László Nyulászi,[a, b] and Tibor Höltzl*[a, b, c]

Here we systematically investigate the CO$_2$ and H$_2$ activation and dissociation on small Cu$_n$Zn$^{0/+}$ (n = 3–6) clusters using Density Functional Theory. We show that Cu$_6$Zn is a superatom, displaying an increased HOMO-LUMO gap and is inert towards CO$_2$ or H$_2$ activation or dissociation. While other neutral clusters weakly activate CO$_2$, the cationic clusters preferentially bind the CO$_2$ in monodentate nonactivated way. Notably, Cu$_4$Zn allows for the dissociation of activated CO$_2$, whereas larger clusters destabilize all activated CO$_2$ binding modes. Conversely, H$_2$ dissociation is favored on all clusters examined, except for Cu$_6$Zn. Cu$_3$Zn$^+$ and Cu$_4$Zn, favor the formation of formate through the H$_2$ dissociation pathway rather than CO$_2$ dissociation. These findings suggest the potential of these clusters as synthetic targets and underscore their significance in the realm of CO$_2$ hydrogenation.

Introduction

Carbon dioxide acts as a greenhouse gas and its high concentration in the atmosphere contributes, among others, to global warming and ocean acidification. Global awareness to take action has led to the Power-to-X approach.[1] in which the synthesis of products (often energy carriers) can be performed by chemical transformations via carbon-free primary energy generation. Consequently, the transformation of CO$_2$ into added-value chemicals presents a remarkable potential to utilize carbon-free electricity as well as to reduce the volume of petrochemical-based reactants required to produce different chemicals[1] such as formic acid or methanol.[2]

The hydrogenation of CO$_2$ to C$_1$ compounds has been carried out by a large number of catalysts in order to overcome the kinetic barrier. Among these, copper-based catalysts are well-known for their high performance in the methanol production.[3,4] In particular, when these copper-based catalysts are accompanied by ZnO, their intrinsic activity towards methanol synthesis increases in an effect known as the Cu–ZnO synergy.[5,6] However, the typical heterogeneous catalysts are highly complex systems, and the understanding of the reaction mechanism and the active sites is often incomplete.

While copper-zinc based catalysts are active for CO$_2$ hydrogenation to methanol, the reaction mechanism is still being actively investigated, and both the zinc oxide interface or the copper-zinc alloy may be the key structures in catalysis.[5,7–13] Recent in-operando studies indicate the first one to be the most important motif. Copper-zinc alloys are also good electrocatalysts. In fact, metallic copper-zinc structures, prepared either directly from metals[14] or by in-situ reduction of CuO/ZnO[15–17] were found to be good electrocatalysts for CO$_2$ electroreduction. A recent operando spectroscopy study has been shown the importance of the zinc to stabilize the Cu(I), relevant for the synthesis of C$_{2+}$ products.[18] On the other hand, galvanically prepared copper-zinc catalysts, in particular with high Zn content, have been shown to catalyze the formation of CO with high Faraday efficiency.[19] Recently, Density Functional Theory (DFT) and Neural Network potential based high throughput screening of CuZn model nanoparticle active sites showed the synergistic effect of the copper-zinc for CO binding, what facilitates the C$_{2+}$ product formation.[20] It has also been concluded using DFT computations that the icosahedral Cu$_{54}$Zn or Cu$_{54}$Cd are optimal for the electrochemical conversion of CO$_2$ to CO.[21]

Gas-phase cluster models might provide valuable insight into the molecular processes in catalysis, as it has been shown e.g. for CO oxidation catalyzed by small gas phase palladium cluster cations.[22] Pd$_n^+$ showed similar reaction paths for this reaction to that on extended surfaces, however the energetics was different, and particularly, Pd$_6^+$ has been shown to be less poisoned by CO.[22] Thus, investigation of metal clusters helps to elucidate the reaction paths, and the understanding of their role in the catalytic process opens the way towards more efficient catalysts. Metal clusters can mimic the active sites of the catalyst and the elementary steps of C$_1$ product formation can be studied at the molecular level.[22–24]

The activation and dissociation of hydrogen plays a central role in the catalytic conversion of CO$_2$ towards valuable compounds. Reaction of gas phase metal hydride anions PtH$_n^-$,[25] PdH$^-$[26] and Cu$_2$H$_2^-$[27] have been investigated experimentally and the formation of formate has been confirmed. DFT computations showed that the hydrogen dissociation on

[a] B. Zamora, Prof. Dr. L. Nyulászi, Dr. T. Höltzl
Department of Inorganic and Analytical Chemistry, Budapest University of Technology and Economics, 1111-Budapest, Műegytem rkp 3 Hungary
E-mail: tibor.holtzl@furukawaelectric.com

[b] Prof. Dr. L. Nyulászi, Dr. T. Höltzl
HUN-REN-BME Computation Driven Chemistry research group, 1111-Budapest, Műegytem rkp. 3 Hungary

[c] Dr. T. Höltzl
Furukawa Electric Institute of Technology, Nanomaterials Science Group, 1158 Budapest Késmárk utca 28/A, Hungary

Supporting information for this article is available on the WWW under https://doi.org/10.1002/cphc.202300409

ChemPhysChem

Research Article
doi.org/10.1002/cphc.202300409

Chemistry
Europe
European Chemical
Societies Publishing

small copper clusters Cu_n (n = 2–15) is favoured thermodynamically and at several cluster sizes also kinetically.[28] The hydrogen dissociation was experimentally demonstrated on small Cu_n^+ (n = 4–7) cationic clusters.[29] Also, the co-adsorption of hydrogen and CO_2 on Cu_n^+ clusters has been reported in a combined experimental and computational investigation,[30] and while hydrogen dissociation was confirmed, CO_2 reduction was not observed. Facile hydrogen dissociation has been computed also in doped clusters, like Cu_nPd,[31] or $Cu_{4-n}Pt_n$ (n = 1–4),[32] while $Cu_{4-n}Au_n$ (n = 1–3) clusters bind hydrogen non-dissociatively.[32] On the other hand, weakly bound hydrogen has been computed on Cu_nZn (n = 1–9) clusters.[33]

Not only can metal clusters provide clean and well-defined model systems to study the different types of active sites in the catalysts, but themselves can also behave active in catalytic processes. For example, the facile CO_2 hydrogenation to methanol was reported by Al_2O_3 supported Cu_4 sub-nano clusters.[24] Here the particle size, composition and also the support has an important role. Alumina-deposited Cu_4 has been shown to exhibit higher turnover rate for CO_2 hydrogenation than Cu_3 or Cu_{20}.[34] In-situ spectroscopy studies show the importance of the support binding of the copper sub-nano clusters for the CO_2 reduction.[35] For CO_2 hydrogenation an optimal cluster size of Cu_{19} has been predicted using DFT computations.[36] It has also been shown that small copper clusters deposited on ZnO are more active catalysts for the CO_2 hydrogenation to CO than the larger particles.[37] Copper sub-nano clusters have also been found to be active in CO_2 hydrogenation in various other surfaces, like Fe_2O_3[38] or TiO_2.[39] Small tetraatomic metal clusters,[40] size selected sub-nano-clusters of first row transition metals[41] and copper clusters supported on boron doped graphene[36] have been predicted by DFT computations, while nitrogen doped graphene supported copper clusters[42] and Cu_5 and Cu_{20} clusters on carbon[43] have been realized experimentally as good electrocatalysts.

To contribute to the understanding of the catalytic mechanism of CO_2 hydrogenation on copper-zinc catalysts, here we study gas-phase zinc-doped copper clusters of different size and their roles in CO_2 and H_2 activation.

Following the work reported on the CO_2 activation mechanism on Cu_3X (X = transition metal atom) neutral clusters,[23] we extended the investigation on the lowest energy isomers of Cu_nZn (n = 4–6), which are within the accessible size-range of cluster reactivity analysis using infrared multi-photon experiments.[44] Up to now only a few neutral Cu_nZn clusters were studied in the literature,[33,45] and these neutral clusters were considered catalysts only in glycerol hydrogenation.[46] We also extend the studies toward the cationic clusters, which are more likely realized in typical gas phase experimental studies.[44] Furthermore, some experimental and theoretical surface studies suggest that the Cu-based active sites for CO_2 hydrogenation to methanol are partially positively charged species,[47,48] while others attribute the catalytic activity to the fully reduced Cu^0 catalyst.[24] Thus, a comparison of the corresponding cationic and neutral Cu_nZn clusters in the CO_2 hydrogenation reaction should provide information on the role of the cationic charge on the activity of the clusters.

While CO_2 dissociation is generally unfavoured on copper surfaces, several small metal clusters are highly active in the C—O bond cleavage, as it is reviewed above. Thus, we investigate both the CO_2 or H_2 adsorption, activation and dissociation on zinc doped copper clusters. We generate the structures having different CO_2 binding modes and determine the reaction paths leading to the low energy isomers. We hope to gain a deeper understanding of the active site properties and the elementary steps in the CO_2 reduction reaction, furthermore, we expect to obtain information on the effects of cluster size.

Computational Details

For the computations, we used the Gaussian 16[49] and Q-Chem 6.0[50] packages. First, we benchmarked the possible functionals and basis sets to select a sufficiently accurate method. The details of the benchmarking are presented in the Supporting Information (Tables S1–S5 and Figures S1–S2). On the basis of these results, and in accordance with some of our previous works,[23,30,51] we selected the hybrid version of the nonempirical meta-generalized gradient approximation (MGGA) TPSS functional (TPSSh)[52] along with def2-TZVP basis set as the method used for the geometry optimizations and to determine the harmonic vibrational frequencies of all structures.

First, we considered the low spin-states. The geometrical structures of the low energy Cu_3Zn isomers were taken from the previous systematic study.[23] For Cu_nZn (n = 4–6), we used the reported structures,[33,45] but carried out further searches by changing the zinc atom position in the cluster. In some cases, further randomly selected structures were also optimized, but all the minima obtained in this manner were of high energy. From the optimized structures, higher spin states were also considered (1 and 3 for even and 2 to 4 for clusters having odd number of electrons, respectively), and the geometries of these spin states were optimized as well.

For the hitherto unknown cationic clusters, initially, we did not carry out a full structural search, but the four lowest-energy neutral clusters were recomputed with a positive charge and apparently different multiplicity to save computer time. In addition, since Cu_n clusters are inherently isoelectronic with $Cu_{n-1}Zn^+$ clusters, we systematically substituted copper with zinc in the previously reported most stable Cu_n structures[45,53,54] and optimized the resulting cationic structures. The optimized structures were re-optimized in the higher spin states. Afterwards, the analytical second derivatives of the molecular energy with respect to the nuclear coordinates were computed on the fully optimized structures to confirm that the minima and transition structures have zero and one imaginary frequency, respectively.

The results obtained from the initial search were compared against the results using the CALYPSO structure prediction method[55,56] based on a particle swarm optimization (PSO) algorithm. Initially, the CALYPSO parameters were 0.8 for the proportion of the structures generated by PSO, and 30 for the population size. However, for Cu_4Zn^+ and Cu_5Zn^+, as they present several low energy isomers, the parameters were tightened to 0.6 for the PSO ratio and 50 for the population size. The results of the CALYPSO structural searches were subsequently compared against the initial search and the global minimum as well as the ordering of the isomers for each size was verified.

Subsequently, to generate inputs for geometry optimization, we used an in-house code as in reference[23] to systematically investigate carbon dioxide and dihydrogen adsorption in different binding modes to low-energy bare metal clusters (up to 25 kJ/mol above our global minimum; see the Results section). In the binding modes considered, CO_2 and H_2 were either activated (indicated by the bending of the CO_2 moiety and by increased bond lengths) or dissociated (the bound CO_2 molecule into CO and O, for H_2 into separated hydrogens). The details of the different binding modes can be found in the SI (Table S7).

To explore the full reaction pathways for the CO_2 and H_2 activation and dissociation reactions, intermediates and products were located for both the neutral and cationic clusters. The Freezing String Method (FSM)[57,58] was used to locate good guesses of the transition structure geometries and the minimum energy pathways connecting the reactant and product structures (i.e. the aforementioned binding modes). This initial guess geometry of the transition structure was further refined using the eigenvector-following method, as implemented in the Q-Chem software.[50] The located first-order saddle point was further verified by ensuring that the imaginary frequency corresponded to the vibrational normal mode of the atoms involved in bond formation or breaking. Once the transition state geometry was located, Intrinsic Reaction Coordinate (IRC) computations were performed to explore the potential energy surface in the vicinity of the transition state and to verify the proposed energy pathway.

The electronic structure analysis was carried out using Energy Decomposition Analysis (EDA),[59] Natural Population Analysis as part of the Natural Bond Orbitals (NBO)[60] package incorporated in Q-Chem.
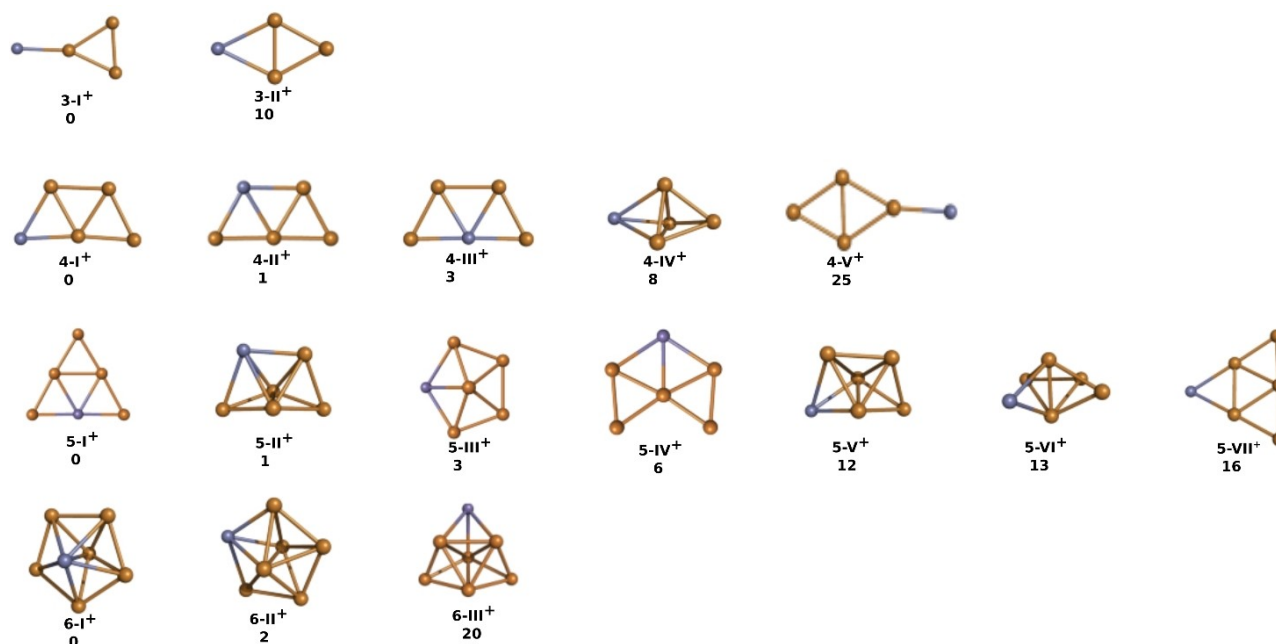
Results and Discussions

Bare Cluster Geometries and Electronic Structures

First, we discuss different optimized Cu_nZn bare cluster geometries (n = 3–6) which are numbered as **N-X** (**N-X**$^+$ for the cationic clusters), where **N** is the number of Cu atoms in the cluster and **X** refers to the number of the given structure in the order of decreasing relative stability (Figures 1 and 2) and analyze their electronic structures, which will serve as a reference for understanding the cluster reactions with CO_2 and H_2.

Our results on the most stable neutral Cu_nZn clusters are shown in Figure 1, while Table S6 in the Supporting Information contains further structural isomers (and their relative energies compared to the lowest energy structure), for both the low and the high-spin state isomers. Figure 1 shows the low energy minima, with energies below +25 kJ/mol (approximately ten times R·T at ambient temperature), with respect to the most stable isomer. The energy gaps to the next stable Cu_nZn n = 4,5 and 6 isomers are 16, 59, and 16 kJ/mol, respectively, and this significant increase in the relative energy further justifies our selection. All the low energy minima had low spin state. Our results for the Cu_nZn (n = 3, 4, 6) neutral clusters were in good agreement with those of previous studies.[33,45] For Cu_5Zn, however, we located a new low-energy minimum (**5-III**), which is only 7 kJ/mol less stable than our global minimum. Cu_3Zn
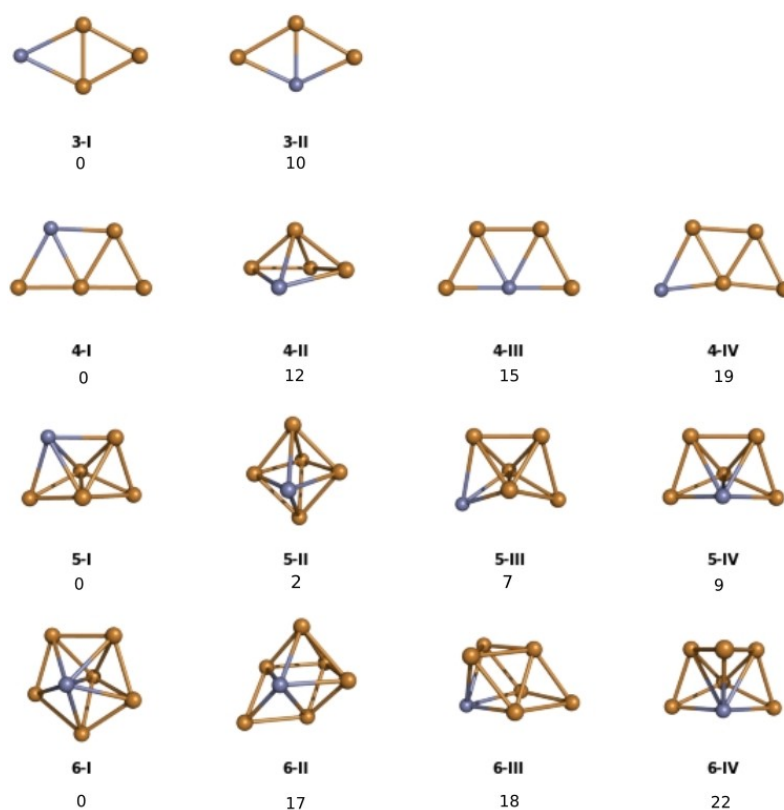
Figure 1. Neutral Cu_nZn (n = 2–6) clusters in the 0–25 kJ/mol range (with respect to the most stable isomer). The spin multiplicities of the Cu_nZn clusters with even n are closed-shell singlets and odd n doublets (TPSSh/def2-TZVP).

ChemPhysChem

Research Article
doi.org/10.1002/cphc.202300409

Chemistry Europe
European Chemical
Societies Publishing

Figure 2. Cationic Cu_nZn (n = 2–6) clusters in the 0–25 kJ/mol range (with respect to the most stable isomer). The spin multiplicities of Cu_nZn^+ clusters with even n are doublets and odd n open-shell singlets. (TPSSh/def2-TZVP).

and Cu_4Zn (but **4-II**) are planar, while Cu_5Zn and Cu_6Zn clusters have three-dimensional (3D) geometries, again in agreement with the previous studies.[33,45]

Cationic Cu_nZn^+ (n = 3..6) clusters again show a low-spin ground state (for odd n closed-shell singlets, for even n doublets). It can be seen from the data presented in Figure 2 that the geometries of Cu_3Zn^+ and Cu_4Zn^+ did not change significantly upon optimization, starting from the neutral structures; and their structures remained planar, and the larger clusters retained the 3D structures. Having noticed, however, that the most stable Cu_6 geometry was planar,[45,53,54] we became curious, whether the analogous planar structure exists for the isoelectronic Cu_5Zn^+ cluster as well. Thus, exchanging systematically one copper atom for zinc (on two different positions) we located two further minima (**5-I⁺** and **5-VII⁺**), with **5-I⁺** being more stable than any of the 3D structures (Figure 2). It is interesting to note that **5-I⁺** exhibits similar triangular geometry with zinc atom residing on one of the edges as the analogous Au_5Zn^+ cluster.[61] While for Cu_3Zn^+ the energy difference between **3-II⁺ and 3-III⁺** is considerably larger than in case of the neutrals, for the Cu_4Zn^+ clusters the energy differences between the four optimized structures are very small. For consistency with the neutrals, isomers lying at most 25 kJ/mol above the lowest energy isomer are presented in Figure 2, and further structures including high-spin states are shown in Table S7 of the Supporting Information. A particular feature of Cu_6Zn is that starting the geometry optimization of the cation from the lowest energy neutral geometry rearranges, whereas the optimization of a neutral starting from the stable Cu_6Zn^+ (**6-II⁺**) geometry yields a new structure, which is 38 kJ/mol above the most stable neutral structure. Interestingly, the most

stable **6-II⁺** could only be optimized from the initial structure provided by CALYPSO.

We characterized the relative stabilities of the lowest energy structures of Cu_nZn neutral and cationic clusters by investigating two measures. First, the relative atomization energy,[67,68] E_a, was derived as the difference between the sum of the total energies of the atoms constituting the cluster ($n \cdot E(Cu) + E(Zn)$) and the total energy of the clusters ($E(Cu_nZn)$). The relative result was obtained by dividing the relative atomization energy by the number of atoms in the cluster ($n + 1$) (Equation 1). The increased relative atomization energy values indicate extended cluster stability.

$$E_a = \frac{n \cdot E(Cu) + E(Zn) - E(Cu_nZn)}{n + 1} \quad (1)$$

A second measure for the stable gas phase cluster formation in an experimental cluster source, whereby a cluster is built up sequentially from individual atoms, is the second-order energy difference: $\Delta^2 E$.[33,62,63] It is defined by Equation 2 as the difference between the energy of Cu_nZn and the energy of the clusters with one more and one fewer Cu atom, thus with reference to its smaller and larger neighbors. A positive value indicates higher cluster stability with respect to the possible "neighbors".
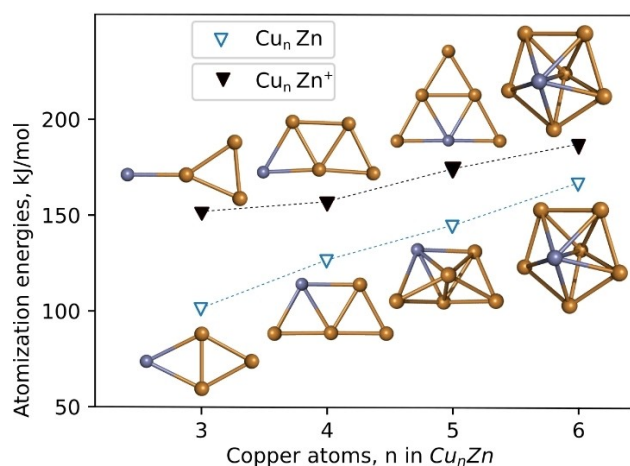
$$\Delta^2 E(n) =$$

$$\Delta^2 E(n) = E(Cu_{n+1}Zn) + E(Cu_{n-1}Zn) - 2E(Cu_nZn) \quad (2)$$

ChemPhysChem

Research Article
doi.org/10.1002/cphc.202300409

Chemistry
Europe
European Chemical
Societies Publishing

Indeed, this approach has been successfully applied in various studies, such as germanium clusters and scandium-doped copper cluster cations, correlating the maxima at certain cluster sizes with peak heights in the experimental mass abundance spectra.[64–66]
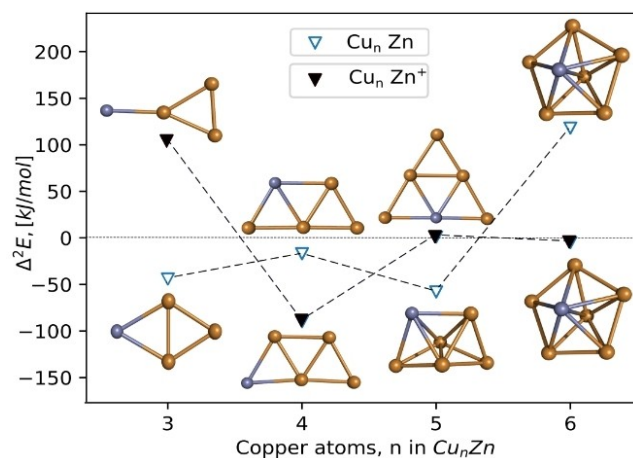
The calculated E_a as a function of the number n of copper atoms is plotted in Figure. 3. For the neutral clusters the atomization energies increase monotonically with the increasing number of the copper atoms, in agreement with the previous results.[33]

For the cationic clusters, we considered both $Cu^+ + Zn$ (closed-shell) and $Cu + Zn^+$ (open-shell) products. Because the closed-shell fragments are more stable by 123 kJ/mol (in reasonable agreement with the 161 kJ/mol difference of the experimental ionization energies of Cu and Zn),[67,68] for the calculation of the atomization energies the decomposition to $Cu^+ + Zn$ is presented in Figure 3.

The cationic Cu_nZn clusters exhibited significantly higher E_a values than their neutral counterparts, indicating increased stability. Although also cations generally become more stable as the size of the cluster increases, this trend is not as consistent as in case of the neutral clusters (see Figure 3). Specifically, there is a larger difference in the relative atomization energy when transitioning from a doublet to a singlet structure, with low-spin Cu_3Zn^+ showing particularly significant stabilization.

According to the second energy differences (Figure 4) for the neutrals, odd cluster sizes ($n_{Cu} = 2,4,6$) are more stable (in agreement with the previous results),[41] whereas in the cationic case, even-sized clusters ($n_{Cu} = 3,5$) show stabilization compared to odd-sized clusters. Again, these trends can be attributed to the presence or absence of unpaired electrons. Altogether, cluster sizes of $n = 3$ for the cationic case and $n = 6$ for the neutral case are clearly more stable than those with other sizes.

The outstanding stability of the neutral Cu_6Zn and cationic Cu_3Zn^+ clusters, as shown by the second energy difference, can be explained using the phenomenological shell model (PSM) of metal clusters.[75,76] According to this model, itinerant electrons delocalize over the cluster and are confined according to their geometrical shape. In the simplest version of PSM, confinement is described using a simple mean field potential, that is, the electrons are modelled as particles in a box. The resulting orbitals have similar shapes to those of the atomic orbitals, and are denoted by capital letters, such as S, P, … In the case of copper and zinc, the valence s electrons are itinerant; thus, in the neutral Cu_6Zn, eight itinerant electrons are present, corresponding to the $1S^2P^6$ closed electronic structure for the compact 3D "quasi-spherically shaped" (Figure 1) Cu_6Zn, explaining its extended stability. The Clemenger-Nilsson model describes the gradual loss of the orbital degeneracy with the distortion of the cluster geometry from the quasi-spherical shape.[69] For the planar, Cu_3Zn^+ (Figure 2) the degeneracy of the P orbitals is lost and P_x (which aligns along the acute apex direction) has considerably lower energy than the P_y (which aligns along the obtuse apex direction) or P_z (which aligns perpendicularly to the plane of the cluster atoms). Thus, the four itinerant electrons in Cu_3Zn^+ have a $1S^2 1P_x^2$ closed shell and stable electronic structure. Similarly, for Cu_4Zn, with six itinerant valence electrons, distorted oblate shape was found and the ordering of the energy levels is given by $1S^2 \{1P_x\ 1P_y\}^4$, where the curly bracket denotes a (quasi)-degeneracy. This is a closed electronic structure of a 2D system. However, it must be noted that Cu_5Zn^+ is a planar, triangle shape cluster with 6 itinerant electrons, which also implies the closed $1S^2 \{1Px\ 1Py\}^4$ electronic structure, similarly to the previously reported σ-aromatic Au_5Zn^+.[61] However, our second energy difference analysis does not show an extended stability for Cu_5Zn^+.

This extended stability is also reflected by the HOMO-LUMO gaps (ΔE_{H-L}). Clusters with large energy HOMO LUMO gaps ($\Delta E_{H-L} > 1.5$ eV) generally behave as *superatoms* capable of preserving their chemical identity and structure,[77,78] i.e. high chemical stability. For example, the tetrahedral Au_{20} cluster exhibits a large HOMO-LUMO gap ($\Delta E_{H-L} = 1.82$ eV calculated, 1.77 eV experimental),[70,71] and among medium-sized 3D metal clusters it is renowned for its high stability. The calculated ΔE_{H-L} for the neutral Cu_6Zn and the cationic Cu_3Zn^+ clusters

Figure 3. Relative atomization energies for the lowest-energy Cu_nZn (n = 1–6) neutral (blue) and Cu_nZn^+ (n = 1–6) cationic (black) clusters. The values were obtained using the TPSSh/def2-TZVP level of theory.

Figure 4. Second energy differences for the lowest energy Cu_nZn (n = 3–6) neutral (blue) and Cu_nZn^+ (n = 3–6) cationic (black) clusters. The values were obtained using the TPSSh/def2-TZVP level of theory.
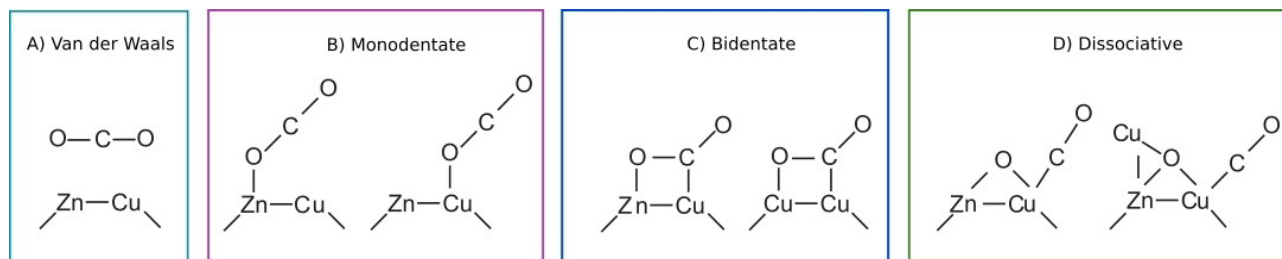
ChemPhysChem

Research Article
doi.org/10.1002/cphc.202300409

Chemistry Europe
European Chemical
Societies Publishing

Scheme 1. CO_2 binding modes. The Zn and Cu atoms represent the adsorbent binding sites in the $Cu_nZn^{0/+}$ clusters.

are of 2.26 eV and 3.32 eV, respectively, significantly surpassing the value for the Au_{20} cluster. Thus, apart from the previously considered[33] Cu_6Zn also the cationic Cu_3Zn^+ cluster should have enhanced stabilities and are therefore possible synthetic targets.

Furthermore, it is important to note that the clusters themselves are fluxional and can undergo rearrangement. This is in line with the recent observation of the fluxionality of several small metal clusters.[72] As shown in Figure S3, there is a small energy barrier of only 25 kJ/mol to reach isomer **4-I** starting from **4-II**.

The charge distribution, especially the localization or delocalization of the positive charge in the clusters, is an interesting question; thus, the natural charges of the lowest-energy isomers were calculated and are shown in Figure S8 of the Supporting Information. For neutrals and cationic clusters, the largest positive charge is in each cluster at Zn, in accordance with its electronegativity, which is lower than for copper. In all cases, the Cu atoms neighboring Zn are less positive (thus, more nucleophilic) than those separated by more than one Cu–Cu bond.

Having investigated the clusters and their stabilities, we considered their possible role in the CO_2 hydrogenation reaction. First, we consider one by one the stability of the different binding modes of the reactants (CO_2 and H_2) with the investigated clusters. The approaching reactant might form a loose complex with the cluster. In accordance with the weak interaction the bonding situation of the reactant remains virtually unchanged. As a result of a stronger interaction, the bonding might be significantly modified (e.g., CO_2 becomes bent, the interatomic distance in dihydrogen increases). Finally, the original bonds of the reactants can break up. The relative stabilities of these binding modes and the activation barriers were investigated by studying the interconnecting transition states. From these studies we can conclude whether the cluster facilitates preferably hydrogen or CO_2 activation.

CO_2 Activation

As it is mentioned in the computational details, the geometries of the CO_2 adducts in different binding modes were systematically generated (see Scheme 1, while the details on the different CO_2 binding modes are discussed in the SI, Section 3, and in Tables S8 and S10. Basis set dependence studies on the relative

stabilities of the Cu_4Zn cluster-CO_2 are presented in Figures S4 and S5). Here, we discuss the possible CO_2 dissociation reaction pathways on neutral Cu_nZn and cationic Cu_nZn^+ (n = 3–6)clusters.

From all the different binding modes obtained, the lowest energy structures can be categorized into four classes: a weak van der Waals cluster-CO_2 complex (**A**), monodentate binding of an intact CO_2 via the O atom (**B**), bidentate binding of an intact but activated CO_2 (having a bent geometry) with O bound preferentially to Zn (note the electronegativities) and C to one of the neighboring Cu atoms (**C**), dissociative adsorption of CO_2 with monodentate bound CO, via its C atom, while the O binding to some (generally three) metal atoms (**D**). In Figure 5, we have collected the energies for the (**A**), (**B**) and (**C**) type binding modes located for the investigated clusters with respect to the (most stable) isolated cluster and separated CO_2
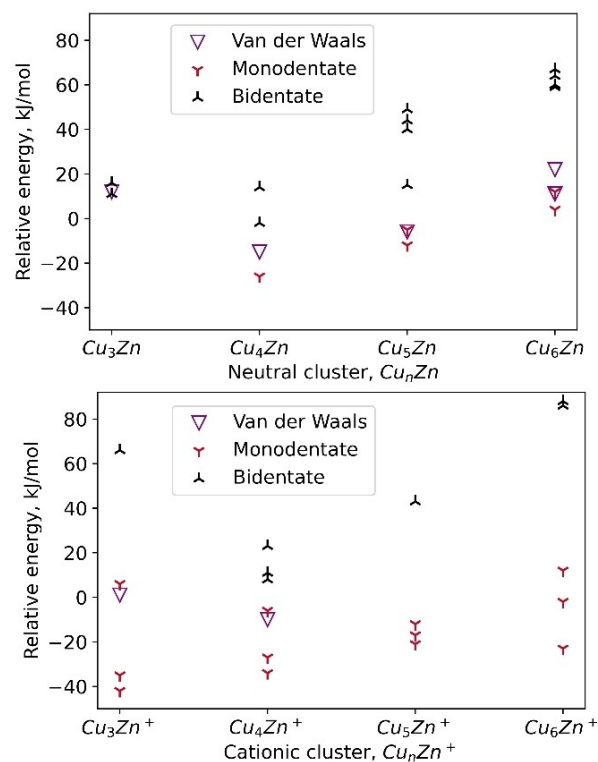
Figure 5. Relative energies of CO_2 adducts with respect to the reactants (most stable bare cluster and CO_2) for binding modes **A**, **B**, and **C** for Cu_nZn (up) and Cu_nZn^+ (down) clusters.

ChemPhysChem

Research Article
doi.org/10.1002/cphc.202300409

Chemistry Europe
European Chemical
Societies Publishing

molecule. The structures of all these adducts are shown in Table S8 in the Supporting Information. While (**A**) and (**B**) type adducts show some degree of stabilization, the (**C**) type bidentate structures are generally higher in energy than the reactants. The energy difference between these structures is small in the case of the smaller clusters Cu_nZn (n = 3,4), while the destabilization of the **C**-type bidentate structures increases for larger clusters. Interestingly, this destabilization was even greater for the cationic clusters. It is important to note that the clusters themselves are fluxional and can undergo rearrangement as was discussed above. This indicates that the same bidentate structure can be obtained from different isomeric clusters. In addition, cluster rearrangement can occur in the presence of CO_2, as shown in Figure S6 of the SI. Thus, the bidentate binding mode observed for **4-I** may not necessarily be characteristic of a single bare cluster structure. In the (**A**) and (**B**) type adducts, the cluster did not show significant affinity towards CO_2. It is worth noting that the cationic clusters have an enhanced affinity towards CO_2 in (**B**) type clusters, as an apparent consequence of their binding with the electronegative oxygen site. In (**C**), the strength of the two-point interactions is counterbalanced by the energy required to bend the linear carbon dioxide system. Because the binding energy is small in all cases, we can expect that the energy required for CO_2 transfer is small, resulting in small barriers between these binding modes. As an example, we located the transition structures that connect the most stable (**A**), (**B**), and (**C**)-type structures in the case of Cu_4Zn and Cu_3Zn^+. In accordance with our expectations, the energy of the transition states connecting the (**B**) and (**C**) type structures did not exceed 15 kJ/mol (Figure S6). Altogether, once the weakly bound van der Waals adduct forms the formation of the (**C**) structures is determined mainly by their relative stability, and for any further reaction we will investigate only the **C** type structures and their possible

rearrangement to the **D** type binding modes, where the CO_2 reactant has decomposed to CO and the cluster-oxide.

It is interesting to note that the stability of the adducts decreased with increasing cluster size. Clearly, the destabilization of the bidentate adducts exceeds approximately 40 kJ/mol for the Cu_nZn clusters with $n \geq 5$ (except one Cu_5Zn **C** type adduct), and it is even larger for the cationic clusters, where the **C**-type CO_2 adducts are destabilized not only for the larger clusters but also in case of Cu_3Zn^+. In addition, both the (translational) entropy contribution to the Gibbs free energy (in particular at higher temperatures) and the Basis Set Superposition Error (BSSE)[73] will further destabilize all adducts. To estimate all these effects, we calculated the counterpoise correction[74] for the series of binding modes of Cu_4Zn (**4-I**), and the data are presented in Table S9 in the SI. While BSSE contributes less than 7 kJ/mol to destabilization, the effect of ZPE is negligible. However, as expected, the entropy contribution to the Gibbs free energy (computed at room temperature and atmospheric pressure, using the Rigid Rotor Harmonic Oscillator Approximation without frequency scaling) is a strong destabilization factor. Thus, the formation of activated CO_2 is possible only for the **C**-type Cu_3Zn, Cu_4Zn, and Cu_4Zn^+ adducts, and for the larger clusters- including that formed with the stable Cu_6Zn - it is energetically unfavored. This suggests that the adduct formation with an activated CO_2 is hindered for larger clusters, and such structures are unlikely to be involved in any subsequent hydrogenation step, due to their small concentration.

To determine which of the energetically available bidentate structures might be involved in a possible reaction with hydrogen, we investigated the bonding structure and extent of CO_2 activation for the most stable (up to 15 kJ/mol) **C**-type Cu_nZn, and Cu_nZn^+ adducts. Table 1 displays these bidentate (**C**-type) CO_2 adducts found for **3-I**, **3-II**, **4-I**, **4-II**, and **V–I**. In the case of Cu_4Zn isomers, the table showcases the two lowest

Table 1. Bidentate CO_2 structures (C type on Scheme 1) on the most stable neutral Cu_3Zn, Cu_4Zn and Cu_5Zn isomers, natural charges, Wiberg bond indices, C–O bond lengths (Å) and O–C–O angles (degrees).[a]

Bidentate CO_2 adduct					
E_{rel} (kJ/mol)	11	16	−2	14	15
Ch_{Zn}	0.49	0.96	0.92	0.51	0.32
Ch_{CO2}	−0.78	−0.90	−1.03	−1.18	−0.62
Wib_{O-Zn}	0.07	0.16	0.16	0.07	0.01
Wib_{Cu-C}	0.33	0.44	0.42	0.56	0.31
Wib_{Cu-Zn}	0.02	0.09	0.11	0.06	0.07
$Wib_{C-O(B2)}$	1.40	1.25	1.27	1.08	1.52

[a] E_{rel}: relative energy with respect to the most stable cluster + CO_2, Ch_{Zn}: Natural charge at Zn [e], Natural charge at the CO_2 moiety [e], Wib_{O-Zn}: O–Zn bond index, Wib_{Cu-C}: Cu–C bond index, Wib_{Cu-Zn}: Cu–Zn bond index, $Wib_{C-O(B2)}$: C–O(B2) bond index.

ChemPhysChem

Research Article
doi.org/10.1002/cphc.202300409
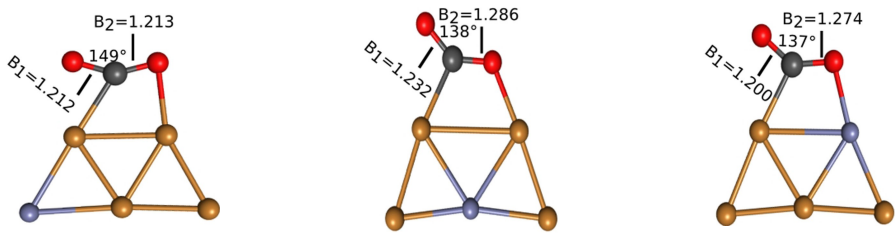
**Chemistry
Europe**
European Chemical
Societies Publishing

energy bidentate structures, and all bare clusters (**4-I** to **4-IV**) form one of these **C**-type adducts. While the structures of the Cu_4Zn and Cu_3Zn moieties remained similar to those of free bare clusters, the structures of the CO_2 adsorbates were significantly different from those of free CO_2. First, the C—O bonds are lengthened from 1.16 Å to 1.31–1.40 Å, indicating weakening, due to the interaction with the clusters. Second, CO_2 bends, with O—C—O angles ranging from 124° to 129°. Besides these geometrical factors, the CO_2 charge is in the range of −0.90 to −1.18, the energy decomposition analysis scheme based on Absolutely Localized Molecular Orbitals (ALMO)[59,75,76] can be used to compute the charge transfer (CT) energy during the adduct formation from the free cluster and the CO_2 molecule, and also to decompose the CT energy into contributions from complementary occupied virtual pairs (Gis) that describe the dominant donor and acceptor orbitals, residing on different fragments of the adduct.[75] The main complementary-occupied-virtual pairs (COVPs) (Figure S9) are presented for each bidentate structure in Table 1. These interacting orbitals clearly indicate partial electron transfer from one of the 1P shell orbitals of the neutral cluster to the antibonding π* orbitals of the CO_2 adsorbates, thus weakening the C—O bond.

The COVP donor is not completely localized on any particular bond, whereas the COVP acceptor is located mainly on the O—C—O bonds. The information is presented in Table 1 and Figure S9 provides valuable insights into the electronic and geometrical factors that contribute to the activation of CO_2 by neutral Cu—Zn clusters, specifically highlighting the central role played by the bidentate structure. Further analysis was conducted to examine the relationship between charge transfer energy and the C—O bond index. The results depicted in Figure S10 show a good correlation, with a coefficient of determination of 0.965.
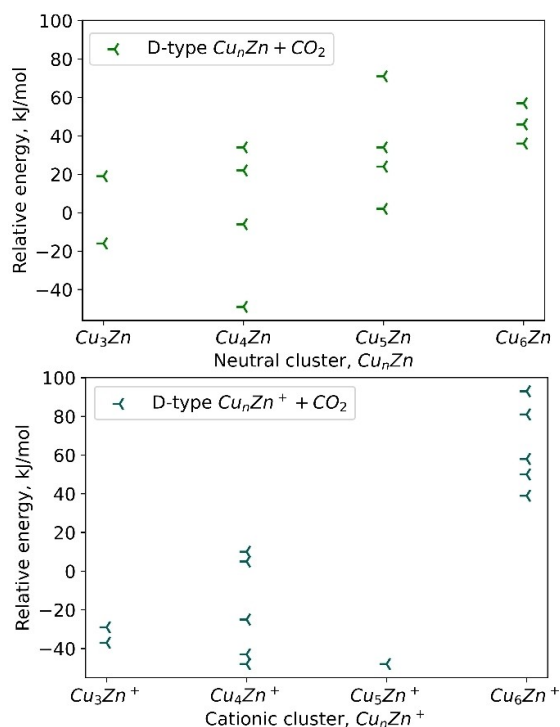
The Cu_4Zn bidentate structure (**C**) with the lowest C—O Wiberg bond index exhibited the highest charge transfer energy, and this increase in the strength of the charge transfer interaction was linked to the activation of CO_2. As shown in Table 1, this structure is not too unstable, only 14 kJ/mol above our minimum energy cluster + CO_2, exhibiting sizeable CO_2 activation. Altogether, the involvement of this structure in a subsequent hydrogenation reaction step cannot be fully excluded. The CO_2 activation by the cationic clusters is smaller than for their neutral counterparts, as it can be seen comparing the data collected in Table 2 with those in Table 1.

Further to the possible hydrogenation of the **C** type bidentate intermediates, it is also of importance, whether C—O bond breaking can take place on the cluster leading to a **D** type binding mode. In these structures the cluster is oxidized, and CO is attached to one of the metal atoms (Scheme 1). Clearly, if the formation of such structures were preferred, upon CO release and subsequent hydrogenation of the cluster oxide (yielding H_2O as byproduct) a catalytic cycle can be envisaged. To this end, we have first investigated the relative stability of the optimized **D** type adducts, for both neutral and cationic clusters, as collected in Figure 6. Likewise, for the **C**-type bidentate structures (see above), the stability of the **D**-type structures decreases with the increasing cluster size. No stable **D**-type Cu_nZnCO_2 structure was found for n = 5 and 6, and for n = 6 also all cationic **D**-type adducts were unstable. In general, the adducts of the neutral clusters are less stable. For the neutrals we found three, while for the cationic system six stable **D** type adducts. To see whether these stable adducts can form from **C** type bidentates, we investigated the transition structures leading in the stable neutral and cationic **D** type structures. The calculated reaction pathways are presented in Figures 7 and 8, for the neutrals and cations, respectively. Clearly, for the small Cu_3Zn clusters the barriers are prohibitive for both neutral and cation. Much smaller barriers were found,

Table 2. Bidentate CO_2 structures (C type on Scheme 1) on the most stable cationic Cu_4Zn^+ isomers their natural charges, Wiberg bond indices, C—O bond lengths (Å) and O—C—O angles (degrees).[a]

Bidentate CO_2 adduct			
E_{rel} (kJ/mol)	8	11	23
Ch_{Zn}	0.26	0.53	0.94
Ch_{CO2}	−0.05	−0.58	−0.66
Wib_{O-Zn}	0.00	0.01	0.13
Wib_{Cu-C}	0.04	0.32	0.31
Wib_{Cu-Zn}	0.09	0.20	0.04
$Wib_{C-O(B2)}$	1.66	1.40	1.36

[a] E_{rel}: relative energy with respect to the most stable cluster + CO_2, Ch_{Zn}: Natural charge at Zn [e], Natural charge at the CO_2 moiety [e], Wib_{O-Zn}: O—Zn bond index, Wib_{Cu-C}: Cu—C bond index, Wib_{Cu-Zn}: Cu—Zn bond index, $Wib_{C-O(B2)}$: C—O(B2) bond index.

ChemPhysChem

Research Article
doi.org/10.1002/cphc.202300409

Chemistry Europe
European Chemical
Societies Publishing

Figure 6. Relative stability of dissociated (**D** type on Scheme 1) Cu_nZn-CO_2 adducts with respect to the lowest energy cluster for each size and free CO_2 (Cluster + CO_2). Structures of the adducts are given in the SI in Table S11. For Cu_3Zn^+, the **3-II**$^+$ isomer forms the same adduct as the **3-III**$^+$ isomer. The CO_2 adducts of all seven isomers of Cu_5Zn^+ converged to the same **D**-type structure.

however, in case of the Cu_4Zn and the cationic Cu_5Zn clusters, thus for these cluster sizes the CO formation seems to be a viable reaction pathway. It should be noted, however, that these cluster sizes show small stability, according to the second order energy differences.

Gas phase computational studies revealed interesting cluster composition-dependent CO_2 activation and dissociation, as (doped) copper clusters like Cu_3X (where X is a first-row transition metal atom)[23] or $Cu_{4-n}Pt_n$,[77] have been shown to be promising candidates for CO_2 activation due to the electron

transfer to its LUMO. While Cu_4 shows a relatively high barrier for CO_2 dissociation,[40] Cu_3X clusters with early transition metal,[23] $Cu_{4-n}Zr_n$[78] (n = 1–3) or Cu_3Pt[77] can even facilitate the dissociation of CO_2. CO_2 activation was also predicted on small Cu–Ni and Cu–Pd clusters by DFT computations, and it was shown that the activation energy of CO_2 dissociation is lower on the pure Cu_4 cluster, than on palladium substituted analogues.[79] DFT computations showed hindered CO_2 dissociation also on $Cu_{4-n}Sn_n$ clusters.[80]

Cluster-size and composition dependent CO_2 activation and dissociation was observed in the case of carbon doped anionic copper clusters.[81] It is worth noting that the CO_2 dissociation route was found to be feasible in the case of larger copper clusters.[82]
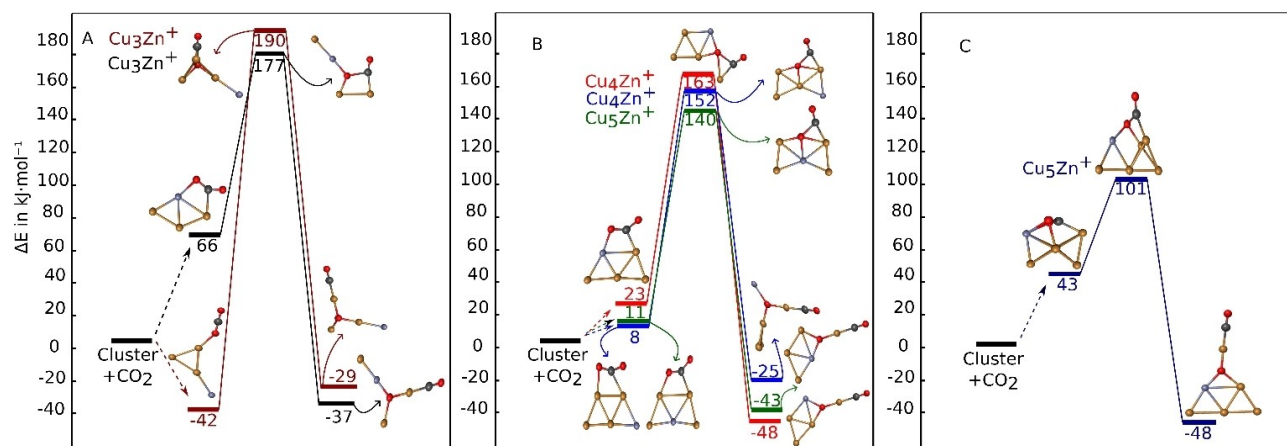
The reported[23] CO_2 dissociation barrier for Cu_4 was compared with our results, and it was found that the activation barrier of CO_2 dissociation on the isoelectronic species, Cu_4 and Cu_3Zn^+ clusters, is very similar and is only reduced by 0.08 eV due to the formal substitution of Cu by the isoelectronic Zn^+. However, the activation barrier of CO_2 dissociation on Cu_3Zn, is reduced by 0.57 eV with respect to the isostructural species Cu_4. The results vary when Cu_3Zn (1.30 eV) is compared to other bimetallic clusters. Cu_3Zr[78] shows a lower energy barrier, 0.13 eV for one of the isomers, whereas Cu_3Pd presents a higher barrier of 1.77 eV.[79]

Altogether, the results of Figures 7 and 8 indicate that, due to the high energy barriers, CO_2 dissociation is hindered on neutral Cu_nZn clusters for n = 3, 5 and 6 and on cationic Cu_nZn^+ clusters for n = 3,4 and 6, while it is feasible on the neutral Cu_4Zn and cationic Cu_5Zn^+ clusters. These clusters are, however, less stable according to the second energy differences, thus their abundance is expected to be small in an experimental cluster source. Also, their decreased stability is expected to lead to structural instabilities upon deposition to surface or at reaction conditions. Thus, there is little hope for their experimental investigation.

For the CO_2 hydrogenation reaction, the alternative pathway is, when the cluster activates dihydrogen first, and the activated adduct reacts then with CO_2. To this end we consider the hydrogen activation by our clusters.
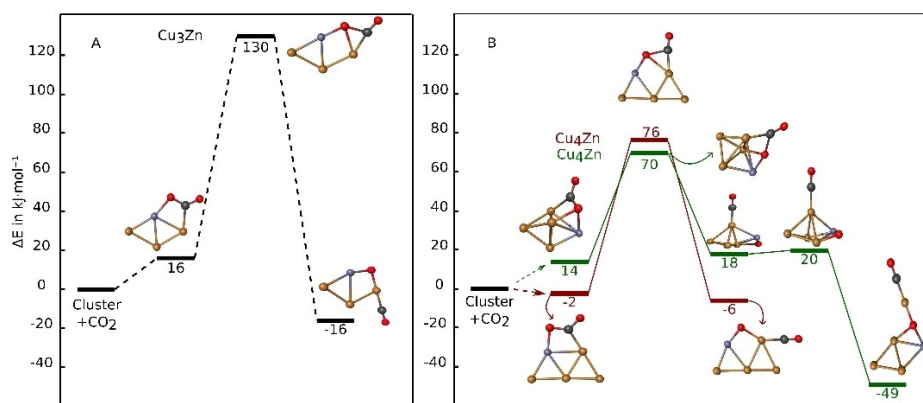
**Figure 7.** Rate-determining steps for the CO_2 dissociation on the neutral Cu_nZn clusters yielding stable products. Panel A: CO_2 + **3-II**, panel B: CO_2 + **4-I** and CO_2 + **4-II**. Relative energies are given with respect to the most stable cluster (our global minimum for the respective size) + free CO_2 molecule.

ChemPhysChem

Research Article
doi.org/10.1002/cphc.202300409

Chemistry
Europe
European Chemical
Societies Publishing

Figure 8. Rate-determining steps for the CO_2 dissociation on the cationic Cu_nZn^+ clusters yielding stable products. Panel **A**: $CO_2 + $**3-I$^+$**, $CO_2 + $**3-III$^+$**, panel **B**: $CO_2 + $**4-I$^+$** and $CO_2 + $**4-II$^+$**, panel C: $CO_2 + $**5-II$^+$** Relative energies are given with respect to the most stable cluster (our global minimum for the respective size) + free CO_2 molecule.

H_2 Activation

First, we present the relative stabilities (with reference to the most stable cluster + free H_2 molecule) of the dissociated $Cu_nZn^{0/+}$-H_2 adducts (Figure 9). The data clearly indicate that hydrogen activation is thermodynamically favoured for all clusters. Thus, the formation of these activated products will be
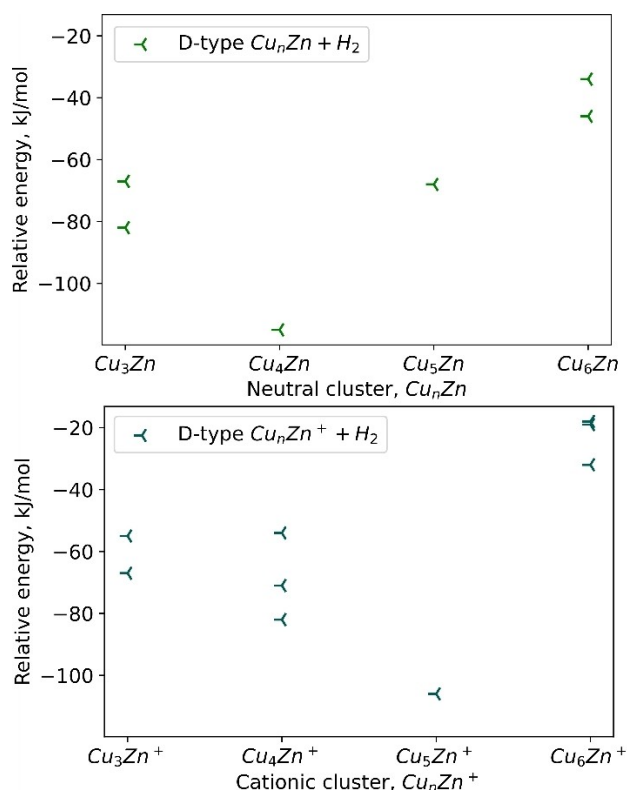
Figure 9. Relative stabilities of dissociated Cu_nZn-H_2 adducts with respect to the lowest energy isomer for each size and free H_2 (Cluster + H_2) for Cu_nZn (top) and Cu_nZn^+ (bottom) clusters. Structures of the adducts are given in the SI in Figure S10. All the isomers of Cu_4Zn, Cu_5Zn, and Cu_5Zn^+ clusters form the same lowest energy **D**-type structure (dissociated H_2).
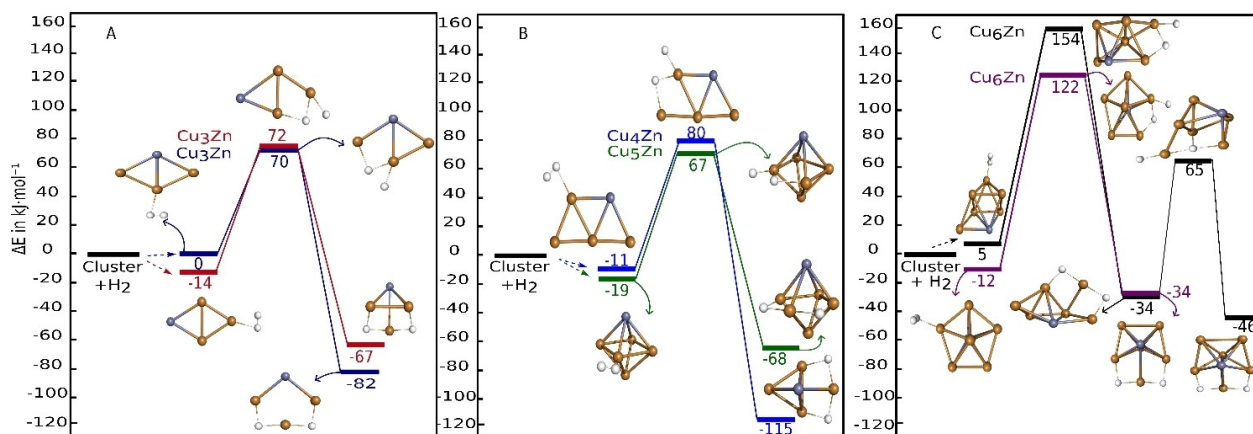
determined by the activation barriers, and accordingly we located transition structures for these processes. As all products are stable, we present the different H_2 dissociation barriers on the neutral and cationic clusters for the most stable products of each cluster size. Figures 10 and 11 show relatively small barriers for all sizes except for neutral Cu_6Zn. The geometries of both the adduct with a dissociated H_2 and that of the transition structure are analogous to those computed for other cluster sizes. However, among the studied cluster sizes, the Cu_6ZnH_2 dissociated product is the least stable, and at the same time the dissociation barrier is the highest. While it is difficult to exclude the existence of other reaction paths with a lower activation energy, the decreased thermodynamic stability of the dissociated H_2 adduct, and the inertness of Cu_6Zn towards the reaction with CO_2 also suggests that this cluster has a decreased reactivity. This is in line with the high stability shown by the second energy differences in Figure 4 and support the superatom character of Cu_6Zn.

For the other clusters, investigated here, the hydrogen dissociation barriers are similar to those computed for the similar sized Cu_n (n = 4–7)[28] or Cu_n^+ (n = 4,5),[29,30] clusters, however higher than that was computed for Cu_9[28] or for Cu_nPd (n = 3–5).[31] It is noteworthy that for Cu_3Zn^+ two similar hydrogen-dissociated adducts differing by the position of the Zn have the same energy (−67 kJ/mol – Table S11)

Overall, as the dissociated H_2 adducts are thermodynamically favoured, and (with the exception of Cu_6Zn) the energy barriers are accessible, the $Cu_nZn^{0/+}$ catalyzed CO_2 hydrogenation is expected to start with the H_2 dissociation.

CO_2 Reduction to Formate

We have investigated the CO_2 reduction to formate via the CO_2 adsorption on Cu_3Zn^+ and Cu_4Zn dissociated hydrogen adducts. The selection of these two cluster sizes was based on their stability, as indicated by the second energy differences. This choice encompassed one neutral cluster and one cationic

ChemPhysChem

Research Article
doi.org/10.1002/cphc.202300409

Chemistry
Europe
European Chemical
Societies Publishing

Figure 10. Rate-determining steps for the H_2 dissociation on neutral Cu_nZn clusters. Panel A: $H_2 + $ **3-II**, panel **B**: $H_2 + $ **4-I** and $H_2 + $ 5-**II**, panel **C**: $H_2 + $ **6-I**. Relative energies are given with respect to the most stable cluster (our global minimum for the respective size) $+ H_2$.
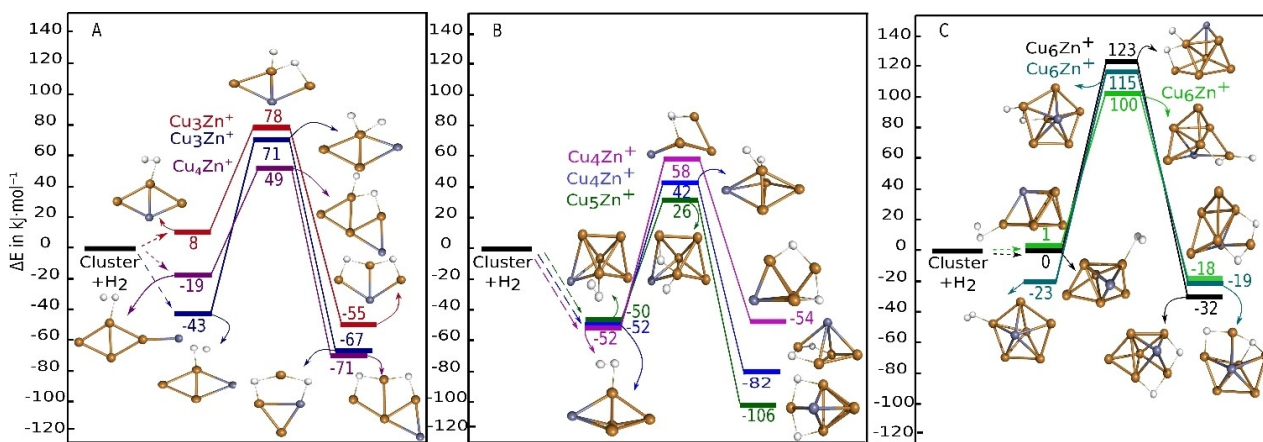
Figure 11. Rate-determining steps for the H_2 dissociation on cationic Cu_nZn^+ clusters. Panel **A**: $H_2 + $ **3-II$^+$**, $H_2 + $ **3-III$^+$**, panel **B**: $H_2 + $ **4-I$^+$**, $H_2 + $ **4-II$^+$**, and $H_2 + $ 5-**V$^+$**. Panel **C**: $H_2 + $ **6-II$^+$**, $H_2 + $ **6-III$^+$**. Relative energies are given with respect to the most stable cluster (our global minimum for the respective size) $+ H_2$.

cluster, with Cu_6Zn excluded due to its reduced reactivity. Additionally, we considered the hydrogen dissociation reaction with the smallest barrier for the respective cluster size. Figure 12 elucidates the rate-determining steps required to produce formate on both clusters.

The reduction of CO_2 to formate on Cu_4^+ clusters was reported to occur with a barrier that is nearly isoenergetic with

Figure 12. Rate-determining steps for the CO_2 reduction to formate on the H_2 dissociated adducts of Cu_4Zn (left) and Cu_3Zn^+ (right) clusters. Relative energies are given with respect to the most stable cluster (our global minimum for the respective size) $+$ the separate H_2 and CO_2 reactants.
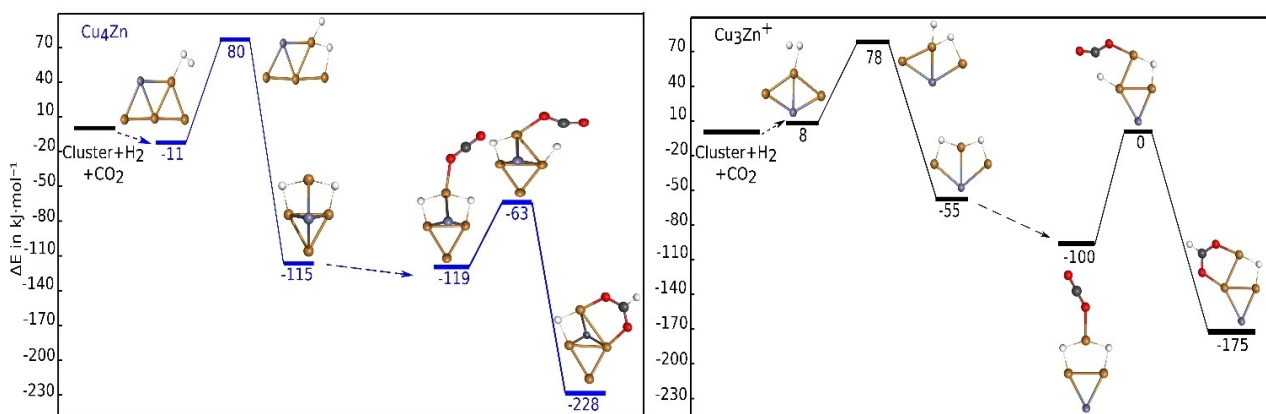
the reactants.[30] In comparison, Cu_3Zn^+ exhibits a similar barrier, resulting in similar energetics for both the reactants and products. Conversely, Cu_4Zn demonstrates a lower barrier for this process. In Figure 12, we illustrate a CO_2 reduction pathway that initiates with H_2 dissociation. Similar to Cu_4^+, one of the hydrogen atoms is transferred to the CO_2 ligand, leading to the formation of the HCOO–Cu_nZn (formate adduct).

Conclusions

Here we investigated the size- and charge-dependent CO_2 and H_2 activation on small $Cu_nZn^{0/+}$ (n=3–6) clusters using Density Functional Theory based methods. The computations showed low spin state for all the stable structures. The global minimum search of the bare cluster structures showed that while clusters in the lower size range are planar, 2D to 3D transition occurs at n=4 and 5 for the neutrals and the cations, respectively. However, low energy isomers were located for all sizes and charge states, indicating a possible fluxional behavior. Indeed, we could locate low energy transition structures for the isomerization, confirming the cluster backbone flexibility. The second energy differences clearly showed the extended stability of Cu_3Zn^+ and Cu_6Zn, suggesting their feasibility as potential synthetic targets. This can be interpreted using the Phenomenological Shell Model of metal clusters, as these clusters have 4 and 8 itinerant electrons, corresponding to $1S_2 1P_x^2$ and $1S^2 1P^6$ closed electronic structures, respectively. Thus, these clusters can be regarded as superatoms, what for Cu_6Zn is further confirmed by its large HOMO-LUMO gap, and also its decreased reactivity with CO_2 or H_2.

We systematically analyzed the CO_2 and H_2 binding to the different clusters. Bidentate CO_2 binding, with bent geometry is possible on neutral clusters, however, its formation is energetically favored only for Cu_4Zn, and the destabilization (with respect to cluster+free CO_2) increases with the increasing cluster size. Also, the bidentate adducts of the cationic clusters are destabilized with respect to their neutral counterparts. Since under thermal conditions the decreased entropy of the adduct is clearly a further destabilizing factor, only some small neutral clusters with activated CO_2 may be available in low concentration for further reaction with dihydrogen. Activation of CO_2 in these clusters is indicated both by the bent geometry, the elongated C–O bond and the decreased Wiberg bond index and also by the partially negative charge of the bound CO_2 molecule. CO_2 preferentially binds to the zinc with its oxygen, and to the adjacent copper with the carbon, which is explained by the partially positive charge of the Zn atom.

Not only the bidentate binding mode, but also the CO_2 dissociation on the clusters shows cluster-size dependence, again the stability of these structures decreases with the increasing cluster size, and neither for Cu_6Zn nor for Cu_6Zn^+ could stable CO_2 dissociated adduct be optimized. Since for the stable dissociated adducts the dissociation barriers were large, we can conclude that CO_2 dissociation (a necessary step for CO formation) is unlikely on Cu_nZn clusters.

Investigation of the dihydrogen reactivity revealed that for all cluster sizes (both cationic and neutral) dissociated binding modes are thermodynamically stable, and relatively low activation barriers exist, except for the case of Cu_6Zn.

H_2 dissociation can take place on most of the studied cases, thus we used the clusters with dissociated hydrogens as starting points to investigate the reduction of CO_2. We demonstrated that for small clusters like Cu_3Zn^+ and Cu_4Zn, the formation of formate by this pathway is more favorable than CO_2 dissociation. These results suggest their suitability as potential synthetic targets and underscore their significance in the context of CO_2 hydrogenation.

Altogether, the results suggest that CO_2 hydrogenation on $Cu_nZn^{0/+}$ (n=3–6) should start with H_2 dissociation. Building upon this insight, the extension of this study to encompass anionic clusters offers a promising opportunity for a comprehensive understanding of the reactivity of Cu_nZn clusters.

Author Contributions

Conceptualization of work: T. H.; Computation: B. Z. Y.; Data analyses: B.Z.Y., L.N., T.H.; Data dissemination & graphics: B.Z.Y.; Writing of manuscript: B.Z.Y., L.N., T.H.; Project support: L.N., T.H.; All authors have read and agreed to the published version of the manuscript.

Supporting Information

The authors have cited additional references within the Supporting Information.[83–87]

Conflict of Interests

The authors declare no conflict of interest.

Data Availability Statement

The data that support the findings of this study are available from the corresponding author upon reasonable request.

ChemPhysChem

Research Article
doi.org/10.1002/cphc.202300409

Chemistry Europe
European Chemical
Societies Publishing

[1] N. W. Kinzel, C. Werlé, W. Leitner, *Angew. Chem. Int. Ed.* **2021**, *60*, 11628–11686.

[2] J. Klankermayer, S. Wesselbaum, K. Beydoun, W. Leitner, *Angew. Chem. Int. Ed.* **2016**, *55*, 7296–7343.

[3] K. C. Waugh, *Catal. Today* **1992**, *15*, 51–75.

[4] K. M. K. Yu, I. Curcic, J. Gabriel, S. C. E. Tsang, *ChemSusChem* **2008**, *1*, 893–899.

[5] S. Kattel, P. J. Ramírez, J. G. Chen, J. A. Rodriguez, P. Liu, *Science* **2017**, *355*, 1296–1299.

[6] M. Behrens, F. Studt, I. Kasatkin, S. Kühl, M. Hävecker, F. Abild-Pedersen, S. Zander, F. Girgsdies, P. Kurr, B.-L. Kniep, M. Tovar, R. W. Fischer, J. K. Nørskov, R. Schlögl, *Science* **2012**, *336*, 893–897.

[7] A. Beck, M. Zabilskiy, M. A. Newton, O. Safonova, M. G. Willinger, J. A. van Bokhoven, *Nat. Catal.* **2021**, *4*, 488–497.

[8] J. B. Wagner, P. L. Hansen, A. M. Molenbroek, H. Topsøe, B. S. Clausen, S. Helveg, *J. Phys. Chem. B* **2003**, *107*, 7753–7758.

[9] E. Frei, A. Gaur, H. Lichtenberg, L. Zwiener, M. Scherzer, F. Girgsdies, T. Lunkenbein, R. Schlögl, *ChemCatChem* **2020**, *12*, 4029–4033.

[10] M. Zabilskiy, V. L. Sushkevich, D. Palagin, M. A. Newton, F. Krumeich, J. A. van Bokhoven, *Nat. Commun.* **2020**, *11*, 2409.

[11] J. Nakamura, T. Fujitani, S. Kuld, S. Helveg, I. Chorkendorff, J. Sehested, *Science* **2017**, *357*, eaan8074.

[12] J. Nakamura, Y. Choi, T. Fujitani, *Top. Catal.* **2003**, *22*, 277–285.

[13] T. Reichenbach, K. Mondal, M. Jäger, T. Vent-Schmidt, D. Himmel, V. Dybbert, A. Bruix, I. Krossing, M. Walter, M. Moseler, *J. Catal.* **2018**, *360*, 168–174.

[14] Y. Baek, H. Song, D. Hong, S. Wang, S. Lee, Y.-C. Joo, G.-D. Lee, J. Oh, *J. Mater. Chem. A* **2022**, *10*, 9393–9401.

[15] D. Ren, J. Gao, L. Pan, Z. Wang, J. Luo, S. M. Zakeeruddin, A. Hagfeldt, M. Grätzel, *Angew. Chem. Int. Ed.* **2019**, *58*, 15036–15040.

[16] D. Ren, B. S.-H. Ang, B. S. Yeo, *ACS Catal.* **2016**, *6*, 8239–8247.

[17] Y. Feng, Z. Li, H. Liu, C. Dong, J. Wang, S. A. Kulinich, X. Du, *Langmuir* **2018**, *34*, 13544–13549.

[18] M. Rüscher, A. Herzog, J. Timoshenko, H. S. Jeon, W. Frandsen, S. Kühl, B. R. Cuenya, *Catal. Sci. Technol.* **2022**, *12*, 3028–3043.

[19] L. Wang, H. Peng, S. Lamaison, Z. Qi, D. M. Koshy, M. B. Stevens, D. Wakerley, J. A. Zamora Zeledón, L. A. King, L. Zhou, Y. Lai, M. Fontecave, J. Gregoire, F. Abild-Pedersen, T. F. Jaramillo, C. Hahn, *Chem Catal.* **2021**, *1*, 663–680.

[20] S. Zhen, G. Zhang, D. Cheng, H. Gao, L. Li, X. Lin, Z. Ding, Z.-J. Zhao, J. Gong, *Angew. Chem. Int. Ed.* **2022**, *61*, e202201913.

[21] A. G. Nabi, Aman-ur-Rehman, A. Hussain, G. A. Chass, D. Di Tommaso, *Nanomaterials.* **2023**, *13*, 87.

[22] S. M. Lang, T. M. Bernhardt, *Phys. Chem. Chem. Phys.* **2012**, *14*, 9255–9269.

[23] M. Szalay, D. Buzsáki, J. Barabás, E. Faragó, E. Janssens, L. Nyulászi, T. Höltzl, *Phys. Chem. Chem. Phys.* **2021**, *23*, 21738–21747.

[24] C. Liu, B. Yang, E. Tyo, S. Seifert, J. De Bartolo, B. von Issendorff, P. Zapol, S. Vajda, L. A. Curtiss, *J. Am. Chem. Soc.* **2015**, *137*, 8676–8679.

[25] X. Zhang, G. Liu, K.-H. Meiwes-Broer, G. Ganteför, K. Bowen, *Angew. Chem. Int. Ed.* **2016**, *55*, 9644–9647.

[26] G. Liu, Z. Zhu, M. Marshall, M. Blankenhorn, K. H. Bowen, *J. Phys. Chem. A* **2021**, *125*, 1747–1753.

[27] Y.-Z. Liu, L.-X. Jiang, X.-N. Li, L.-N. Wang, J.-J. Chen, S.-G. He, *J. Phys. Chem. C* **2018**, *122*, 19379–19384.

[28] G. H. Guvelioglu, P. Ma, X. He, R. C. Forrey, H. Cheng, *Phys. Rev. Lett.* **2005**, *94*, 026103.

[29] O. V. Lushchikova, H. Tahmasbi, S. Reijmer, R. Platte, J. Meyer, J. M. Bakker, *J. Phys. Chem. A* **2021**, *125*, 2836–2848.

[30] O. V. Lushchikova, M. Szalay, H. Tahmasbi, L. B. F. Juurlink, J. Meyer, T. Höltzl, J. M. Bakker, *Phys. Chem. Chem. Phys.* **2021**, *23*, 26661–26673.

[31] P. L. Rodríguez-Kessler, P. Alonso-Dávila, P. Navarro-Santos, J. A. Morato-Márquez, F. Ortíz-Chi, A. R. Rodríguez-Domínguez, *J. Phys. Chem. C* **2019**, *123*, 15834–15840.

[32] L. E. Gálvez-González, J. A. Alonso, L. O. Paz-Borbón, A. Posada-Amarillas, *J. Phys. Chem. C* **2019**, *123*, 30768–30780.

[33] R. Singh, P. Biswas, P. K. Jha, *Int. J. Quantum Chem.* **2020**, *120*, DOI 10.1002/qua.26239.

[34] B. Yang, C. Liu, A. Halder, E. C. Tyo, A. B. F. Martinson, S. Seifert, P. Zapol, L. A. Curtiss, S. Vajda, *J. Phys. Chem. C* **2017**, *121*, 10406–10412.

[35] A. Halder, C. Lenardi, J. Timoshenko, A. Mravak, B. Yang, L. K. Kolipaka, C. Piazzoni, S. Seifert, V. Bonačić-Koutecký, A. I. Frenkel, P. Milani, S. Vajda, *ACS Catal.* **2021**, *11*, 6210–6224.

[36] B. Barhács, E. Janssens, T. Höltzl, *Phys. Chem. Chem. Phys.* **2022**, *24*, 21417–21426.

[37] A. Karelovic, P. Ruiz, *Catal. Sci. Technol.* **2015**, *5*, 869–881.

[38] B. Yang, X. Yu, A. Halder, X. Zhang, X. Zhou, G. J. A. Mannie, E. Tyo, M. J. Pellin, S. Seifert, D. Su, S. Vajda, *ACS Sustainable Chem. Eng.* **2019**, *7*, 14435–14442.

[39] S. K. Iyemperumal, N. A. Deskins, *Phys. Chem. Chem. Phys.* **2017**, *19*, 28788–28807.

[40] C. Liu, H. He, P. Zapol, L. A. Curtiss, *Phys. Chem. Chem. Phys.* **2014**, *16*, 26584–26599.

[41] R. K. Raju, P. Rodriguez, E. N. Brothers, *Phys. Chem. Chem. Phys.* **2023**, *25*, 11630–11652.

[42] X. Su, Z. Jiang, J. Zhou, H. Liu, D. Zhou, H. Shang, X. Ni, Z. Peng, F. Yang, W. Chen, Z. Qi, D. Wang, Y. Wang, *Nat. Commun.* **2022**, *13*, 1322.

[43] R. Passalacqua, S. Parathoner, G. Centi, A. Halder, E. C. Tyo, B. Yang, S. Seifert, S. Vajda, *Catal. Sci. Technol.* **2016**, *6*, 6977–6985.

[44] A. Fielicke, *Chem. Soc. Rev.* **2023**, *52*, 3778–3841.

[45] Q. Liu, L. Cheng, *J. Alloys Compd.* **2019**, *771*, 762–768.

[46] R. Singh, P. Biswas, P. K. Jha, *ACS Omega* **2022**, *7*, 33629–33636.

[47] S. Natesakhawat, J. W. Lekse, J. P. Baltrus, P. R. Ohodnicki Jr., B. H. Howard, X. Deng, C. Matranga, *ACS Catal.* **2012**, *2*, 1667–1676.

[48] J. Szanyi, D. W. Goodman, *Catal. Lett.* **1991**, *10*, 383–390.

[49] M. J. Frisch, G. W. Trucks, H. B. Schlegel, G. E. Scuseria, M. A. Robb, J. R. Cheeseman, G. Scalmani, V. Barone, G. A. Petersson, H. Nakatsuji, X. Li, M. Caricato, A. V. Marenich, J. Bloino, B. G. Janesko, R. Gomperts, B. Mennucci, H. P. Hratchian, J. V. Ortiz, A. F. Izmaylov, J. L. Sonnenberg, Williams, F. Ding, F. Lipparini, F. Egidi, J. Goings, B. Peng, A. Petrone, T. Henderson, D. Ranasinghe, V. G. Zakrzewski, J. Gao, N. Rega, G. Zheng, W. Liang, M. Hada, M. Ehara, K. Toyota, R. Fukuda, J. Hasegawa, M. Ishida, T. Nakajima, Y. Honda, O. Kitao, H. Nakai, T. Vreven, K. Throssell, J. A. Montgomery Jr., J. E. Peralta, F. Ogliaro, M. J. Bearpark, J. J. Heyd, E. N. Brothers, K. N. Kudin, V. N. Staroverov, T. A. Keith, R. Kobayashi, J. Normand, K. Raghavachari, A. P. Rendell, J. C. Burant, S. S. Iyengar, J. Tomasi, M. Cossi, J. M. Millam, M. Klene, C. Adamo, R. Cammi, J. W. Ochterski, R. L. Martin, K. Morokuma, O. Farkas, J. B. Foresman, D. J. Fox, **2016**.

[50] E. Epifanovsky, A. T. B. Gilbert, X. Feng, J. Lee, Y. Mao, N. Mardirossian, P. Pokhilko, A. F. White, M. P. Coons, A. L. Dempwolff, Z. Gan, D. Hait, P. R. Horn, L. D. Jacobson, I. Kaliman, J. Kussmann, A. W. Lange, K. U. Lao, D. S. Levine, J. Liu, S. C. McKenzie, A. F. Morrison, K. D. Nanda, F. Plasser, D. R. Rehn, M. L. Vidal, Z.-Q. You, Y. Zhu, B. Alam, B. J. Albrecht, A. Aldossary, E. Alguire, J. H. Andersen, V. Athavale, D. Barton, K. Begam, A. Behn, N. Bellonzi, Y. A. Bernard, E. J. Berquist, H. G. A. Burton, A. Carreras, K. Carter-Fenk, R. Chakraborty, A. D. Chien, K. D. Closser, V. Cofer-Shabica, S. Dasgupta, M. de Wergifosse, J. Deng, M. Diedenhofen, H. Do, S. Ehlert, P.-T. Fang, S. Fatehi, Q. Feng, T. Friedhoff, J. Gayvert, Q. Ge, G. Gidofalvi, M. Goldey, J. Gomes, C. E. González-Espinoza, S. Gulania, A. O. Gunina, M. W. D. Hanson-Heine, P. H. P. Harbach, A. Hauser, M. F. Herbst, M. Hernández Vera, M. Hodecker, Z. C. Holden, S. Houck, X. Huang, K. Hui, D. C. Huynh, M. Ivanov, Á. Jász, H. Ji, H. Jiang, B. Kaduk, S. Kähler, K. Khistyaev, J. Kim, G. Kis, P. Klunzinger, Z. Koczor-Benda, J. H. Koh, D. Kosenkov, L. Koulias, T. Kowalczyk, C. M. Krauter, K. Kue, A. Kunitsa, T. Kus, I. Ladjánszki, A. Landau, K. V. Lawler, D. Lefrancois, S. Lehtola, R. R. Li, Y.-P. Li, J. Liang, M. Liebenthal, H.-H. Lin, Y.-S. Lin, F. Liu, K.-Y. Liu, M. Loipersberger, A. Luenser, A. Manjanath, P. Manohar, E. Mansoor, S. F. Manzer, S.-P. Mao, A. V. Marenich, T. Markovich, S. Mason, S. A. Maurer, P. F. McLaughlin, M. F. S. J. Menger, J.-M. Mewes, S. A. Mewes, P. Morgante, J. W. Mullinax, K. J. Oosterbaan, G. Paran, A. C. Paul, S. K. Paul, F. Pavošević, Z. Pei, S. Prager, E. I. Proynov, Á. Rák, E. Ramos-Cordoba, B. Rana, A. E. Rask, A. Rettig, R. M. Richard, F. Rob, E. Rossomme, T. Scheele, M. Scheurer, M. Schneider, N. Sergueev, S. M. Sharada, W. Skomorowski, D. W. Small, C. J. Stein, Y.-C. Su, E. J. Sundstrom, Z. Tao, J. Thirman, G. J. Tornai, T. Tsuchimochi, N. M. Tubman, S. P. Veccham, O. Vydrov, J. Wenzel, J. Witte, A. Yamada, K. Yao, S. Yeganeh, S. R. Yost, A. Zech, I. Y. Zhang, X. Zhang, Y. Zhang, D. Zuev, A. Aspuru-Guzik, A. T. Bell, N. A. Besley, K. B. Bravaya, B. R. Brooks, D. Casanova, J.-D. Chai, S. Coriani, C. J. Cramer, G. Cserey, A. E. DePrince, R. A. DiStasio, A. Dreuw, B. D. Dunietz, T. R. Furlani, W. A. Goddard, S. Hammes-Schiffer, T. Head-Gordon, W. J. Hehre, C.-P. Hsu, T.-C. Jagau, Y. Jung, A. Klamt, J. Kong, D. S. Lambrecht, W. Liang, N. J. Mayhall, C. W. McCurdy, J. B. Neaton, C. Ochsenfeld, J. A. Parkhill, R. Peverati, V. A. Rassolov, Y. Shao, L. V. Slipchenko, T. Stauch, R. P. Steele, J. E. Subotnik, A. J. W. Thom, A. Tkatchenko, D. G. Truhlar, T. Van Voorhis, T. A. Wesolowski, K. B. Whaley, H. L. Woodcock, P. M. Zimmerman, S. Faraji, P. M. W. Gill, M. Head-Gordon, J. M. Herbert, A. I. Krylov, *J. Chem. Phys.* **2021**, *155*, 084801.

[51] G. Hou, E. Faragó, D. Buzsáki, L. Nyulászi, T. Höltzl, E. Janssens, *Angew. Chem. Int. Ed.* **2021**, *60*, 4756–4763.

[52] S. Kossmann, B. Kirchner, F. Neese, *Mol. Phys.* **2007**, *105*, 2049–2071.

[53] P. Jaque, A. Toro-Labbé, *J. Chem. Phys.* **2002**, *117*, 3208–3218.

[54] D. Die, B.-X. Zheng, L.-Q. Zhao, Q.-W. Zhu, Z.-Q. Zhao, *Sci. Rep.* **2016**, *6*, 31978.

[55] J. Lv, Y. Wang, L. Zhu, Y. Ma, *J. Chem. Phys.* **2012**, *137*, 084104.

[56] Y. Wang, J. Lv, L. Zhu, Y. Ma, *Comput. Phys. Commun.* **2012**, *183*, 2063–2070.

[57] S. Mallikarjun Sharada, P. M. Zimmerman, A. T. Bell, M. Head-Gordon, *J. Chem. Theory Comput.* **2012**, *8*, 5166–5174.

[58] A. Behn, P. M. Zimmerman, A. T. Bell, M. Head-Gordon, *J. Chem. Phys.* **2011**, *135*, 224108.

[59] R. Z. Khaliullin, E. A. Cobar, R. C. Lochan, A. T. Bell, M. Head-Gordon, *J. Phys. Chem. A* **2007**, *111*, 8753–8765.

[60] E. D. Glendening, C. R. Landis, F. Weinhold, *WIREs Comput. Mol. Sci.* **2012**, *2*, 1–42.

[61] H. Tanaka, S. Neukermans, E. Janssens, R. E. Silverans, P. Lievens, *J. Am. Chem. Soc.* **2003**, *125*, 2862–2863.

[62] C.-G. Li, Z.-G. Shen, Y.-F. Hu, Y.-N. Tang, W.-G. Chen, B.-Z. Ren, *Sci. Rep.* **2017**, *7*, 1345.

[63] J. Barabás, T. Höltzl, *J. Phys. Chem. A* **2016**, *120*, 8862–8870.

[64] W. Schulze, B. Winter, I. Goldenfeld, *J. Chem. Phys.* **1987**, *87*, 2402–2403.

[65] T. Höltzl, N. Veldeman, J. De Haeck, T. Veszprémi, P. Lievens, M. T. Nguyen, *Chem. Weinh. Bergstr. Ger.* **2009**, *15*, 3970–3982.

[66] J. Wang, G. Wang, J. Zhao, *Phys. Rev. B* **2001**, *64*, DOI 10.1103/PhysRevB.64.205411.

[67] X. Liu, X. Xiong, in *Encycl. Geochem. Compr. Ref. Source Chem. Earth* (Ed.: W. M. White), Springer International Publishing, Cham, **2018**, pp. 303–305.

[68] J. Brugger, in *Encycl. Geochem. Compr. Ref. Source Chem. Earth* (Ed.: W. M. White), Springer International Publishing, Cham, **2018**, pp. 1521–1524.

[69] W. D. Knight, K. Clemenger, W. A. de Heer, W. A. Saunders, M. Y. Chou, M. L. Cohen, *Phys. Rev. Lett.* **1984**, *52*, 2141–2143.

[70] Y. Gao, S. Bulusu, X. C. Zeng, *J. Am. Chem. Soc.* **2005**, *127*, 15680–15681.

[71] J. Li, X. Li, H.-J. Zhai, L.-S. Wang, *Science* **2003**, *299*, 864–867.

[72] H. Zhai, A. N. Alexandrova, *ACS Catal.* **2017**, *7*, 1905–1911.

[73] S. Simon, M. Duran, J. J. Dannenberg, *J. Chem. Phys.* **1996**, *105*, 11024–11031.

[74] S. F. Boys, F. Bernardi, *Mol. Phys.* **1970**, *19*, 553–566.

[75] R. Z. Khaliullin, A. T. Bell, M. Head-Gordon, *J. Chem. Phys.* **2008**, *128*, 184112.

[76] S. P. Veccham, J. Lee, Y. Mao, P. R. Horn, M. Head-Gordon, *Phys. Chem. Chem. Phys.* **2021**, *23*, 928–943.

[77] L. E. Gálvez-González, J. O. Juárez-Sánchez, R. Pacheco-Contreras, I. L. Garzón, L. O. Paz-Borbón, A. Posada-Amarillas, *Phys. Chem. Chem. Phys.* **2018**, *20*, 17071–17080.

[78] Megha, K. Mondal, T. K. Ghanty, A. Banerjee, *J. Phys. Chem. A* **2021**, *125*, 2558–2572.

[79] A. Alvarez-Garcia, E. Flórez, A. Moreno, C. Jimenez-Orozco, *J. Mol. Catal.* **2020**, *484*, 110733.

[80] A. Muthuperiyanayagam, A. G. Nabi, Q. Zhao, Aman-ur-Rehman, D. D. Tommaso, *Phys. Chem. Chem. Phys.* **2023**, *25*, 13429–13441.

[81] O. V. Lushchikova, M. Szalay, T. Höltzl, J. M. Bakker, *Faraday Discuss.* **2023**, *242*, 252–268.

[82] X. Zhang, J. X. Liu, B. Zijlstra, I. A. W. Filot, Z. Zhou, S. Sun, E. J. M. Hensen, *Nano Energy* **2018**, *43*, 200–209.

[83] M. Szalay, D. Buzsáki, J. Barabás, E. Faragó, E. Janssens, L. Nyulászi, T. Höltzl, *Phys. Chem. Chem. Phys.* **2021**, *23*, 21738–21747.

[84] R. H. Duncan Lyngdoh, H. F. Schaefer, R. B. King, *Chem. Rev.* **2018**, *118*, 11626–11706.

[85] F. Meyer, Y.-M. Chen, P. B. Armentrout, *J. Am. Chem. Soc.* **1995**, *117*, 4071–4081.

[86] Y.-R. Luo, *Comprehensive Handbook of Chemical Bond Energies*, CRC Press, Boca Raton, **2007**.

[87] A. Haaland, J. C. Green, G. S. McGrady, A. J. Downs, E. Gullo, M. J. Lyall, J. Timberlake, A. V. Tutukin, H. V. Volden, K.-A. Østby, *Dalton Trans.* **2003**, 4356–4366.